Geophysical Journal International

Geophys. J. Int. (2016) **205,** 548–561 doi: 10.1093/gji/ggw038

GJI Mineral physics, rheology, heat flow and volcanology

The influence of normal stress and sliding velocity on the frictional behaviour of calcite at room temperature: insights from laboratory experiments and microstructural observations

B.M. Carpenter,[1,*] C. Collettini,[1,2] C. Viti[3] and A. Cavallo[1]

[1] *Istituto Nazionale di Geofisica e Vulcanologia, Roma, Italia. E-mail: brettmcarpenter@gmail.com*

[2] *Dipartimento di Science della Terra, Sapienza Universita di Roma, Rome, Italy*

[3] *Dipartimento di Scienze Fisiche, della Terra e dell'Ambiente, Università degli Studi di Siena, Siena, Italy*

Accepted 2016 January 21. Received 2016 January 7; in original form 2015 July 9

SUMMARY

The presence of calcite in and near faults, as the dominant material, cement, or vein fill, indicates that the mechanical behaviour of carbonate-dominated material likely plays an important role in shallow- and mid-crustal faulting. To better understand the behaviour of calcite, under loading conditions relevant to earthquake nucleation, we sheared powdered gouge of Carrara Marble, >98 per cent $CaCO_3$, at constant normal stresses between 1 and 100 MPa under water-saturated conditions at room temperature. We performed slide-hold-slide tests, 1–3000 s, to measure the amount of static frictional strengthening and creep relaxation, and velocity-stepping tests, 0.1–1000 μm s^{-1}, to evaluate frictional stability. We observe that the rates of frictional strengthening and creep relaxation decrease with increasing normal stress and diverge as shear velocity is increased from 1 to 3000 μm s^{-1} during slide-hold-slide experiments. We also observe complex frictional stability behaviour that depends on both normal stress and shearing velocity. At normal stresses less than 20 MPa, we observe predominantly velocity-neutral friction behaviour. Above 20 MPa, we observe strong velocity-strengthening frictional behaviour at low velocities, which then evolves towards velocity-weakening friction behaviour at high velocities. Microstructural analyses of recovered samples highlight a variety of deformation mechanisms including grain size reduction and localization, folding of calcite grains and fluid-assisted diffusion mass transfer processes promoting the development of calcite nanograins in the highly deformed portions of the experimental fault. Our combined analyses indicate that calcite fault gouge transitions from brittle to semi-brittle behaviour at high normal stress and slow sliding velocities. This transition has important implications for earthquake nucleation and propagation on faults in carbonate-dominated lithologies.

Key words: Geomechanics; Microstructures; Creep and deformation; Friction; Fault zone rheology; Dynamics and mechanics of faulting.

1 INTRODUCTION

Understanding the physical and chemical processes that control the style of slip on faults in the lithosphere are fundamental problems in earthquake physics and fault mechanics. The slip behaviour of faults, ranging from stable, aseismic creep, to unstable, earthquake rupture exhibits a fundamental control on the types of hazards associated with tectonic plate motion. Significant earthquakes, such as the 1995 Aigion event (Bernard *et al.* 1997), the 2008 Wenchuan earthquake (Burchfiel *et al.* 2008), and events throughout Italy (e.g. Miller *et al.* 2004; Mirabella *et al.* 2008; Govoni *et al.* 2014) have nucleated within or propagated through thick carbonate sequences. These events have shown that carbonate-dominated lithologies can play an important role in mid- to shallow-crustal faulting. Consequently, experimental work focusing on the frictional properties of carbonate-dominated lithologies, under conditions relevant to the shallow crust, has gained prevalence recently (e.g. Verberne *et al.* 2010; Collettini *et al.* 2011; De Paola *et al.* 2011, 2015; Fondriest *et al.* 2013; Scuderi *et al.* 2013; Violay *et al.* 2013; Carpenter *et al.* 2014; Chen *et al.* 2015; Smith *et al.* 2015). These studies, performed over a range of conditions and slip velocities, have highlighted the important role that calcite plays in earthquake nucleation and propagation.

* Now at: School of Geology and Geophysics, University of Oklahoma, Norman, OK, USA.

Deformation experiments on calcite-rich rocks, at velocities consistent with earthquake nucleation, have shown that these materials exhibit frictionally unstable behaviour at conditions pertinent to the shallow crust (e.g. Verberne *et al.* 2010, 2014a,b; Carpenter *et al.* 2014; Tesei *et al.* 2014; Chen *et al.* 2015). Furthermore, some of these studies have highlighted the relatively rapid (Carpenter *et al.* 2014) and sometimes complicated (Chen *et al.* 2015) strengthening behaviour of these materials during laboratory 'interseismic' periods. Most of these studies have been performed at single normal stresses while varying temperature (e.g. Verberne *et al.* 2014b), slip zone complexity (e.g. Carpenter *et al.* 2014) and loading history (e.g. Chen *et al.* 2015). Additionally, some of these studies have identified physico-chemical processes acting in the gouge as primary reasons for the observed behaviour. Such processes include the formation of calcite nanograins leading to crystal plastic behaviour (Verberne *et al.* 2013, 2014a) and active solution/transfer processes that lead to increased strength after hold periods (Chen *et al.* 2015). Furthermore, previous work has confirmed the role of fluids and fluid composition on the mechanical behaviour of calcite at room temperature (Rutter 1974; Zhang & Spiers 2005). Zhang & Spiers (2005) showed that compaction of water-saturated calcite at room temperature was accomplished via pressure solution. They found that fluids meant to restrict (silicone oil) and enhance (0.1 M NaCl) the pressure solution process significantly affected the amount and rate of observed compaction. Room temperature observations of pressure solution in calcite, combined with the decreasing solubility of calcite with increasing temperature (see Plummer *et al.* 1979 for a review) and the fact that the rate of pressure solution in calcite-rich lithologies would be expected to increase gradually to depths of 5–7 km (e.g. Rutter 1983; Gratier *et al.* 2013) indicate that room temperature experiments can provide useful information by capturing this process. Furthermore, increased pore pressure is likely to cause lateral variations in normal stress, not temperature, and will exhibit some control on the mechanical behaviour of the fault. Finally, calcite has been shown to transition between brittle and ductile behaviour at relatively low normal stresses and velocities (e.g. Edmond & Paterson 1972; Fredrich *et al.* 1989; De Bresser *et al.* 2002; Schubnel *et al.* 2006; Brantut *et al.* 2014; Verberne *et al.* 2015). The transition between brittle and ductile behaviour is critical in controlling earthquake source mechanics and the overall strength of the lithosphere (e.g. Byerlee 1968; Scholz 1988; Evans *et al.* 1990). In terms of shear deformation, the end members are well-described by friction and flow laws, respectively. Combined friction/flow laws have been developed (e.g. Shimamoto 1986; Bos & Spiers 2002; Noda & Shimamoto 2010, 2012; Takahashi *et al.* 2011; Verberne *et al.* 2015) to study the transition between these behaviours, that is the semi-brittle field. Relevant studies, that have considered this transition via direct shear experiments, were performed on halite (Shimamoto 1986; Noda & Shimamoto 2010) and calcite (Verberne *et al.* 2015) gouge. Shimamoto (1986) showed a normal stress and velocity dependent roll over in the failure envelope (their fig. 1). This study observed that the normal stress dependent transition towards pressure insensitive strength, that is ductile flow, occurred at lower normal stresses for the slowest velocities. In rate-stepping experiments, Noda & Shimamoto (2010) showed a transition in friction, upon an increasing velocity step, from peak decay to a monotonic increase as the sample transitioned between brittle and ductile deformation. They interpret a monotonic increase in frictional strength upon a velocity step as ductile behaviour and successfully show the ability of a ductile flow law to fit their data. Strain rate dependent transitions between brittle and ductile behaviour in calcite rocks are well known from triaxial experiments (e.g. Rutter 1974).

In order to better understand the mechanical behaviour of calcite at shallow crustal conditions and to expand on current data, we performed experiments over a range of normal stresses, 1–100 MPa, and over 4 magnitudes of slip velocity, tenths of $\mu m\ s^{-1}$ to thousands of $\mu m\ s^{-1}$. Furthermore, we collected post experimental samples for microstructural characterization in order to understand the deformation mechanisms controlling the observed behaviour. Understanding the behaviour of calcite gouge in the semi-brittle field and its implications for earthquake nucleation and propagation are critical to understanding the hazards posed by shallow faults where calcite is the dominant lithology.

2 METHODS

We performed experiments on powdered (grain size $<150\ \mu m$) Carrara marble (>98 per cent $CaCO_3$) under saturated conditions and at room temperature. We saturated our samples with a solution of deionized (DI) water, which had been combined with Carrara marble rubble and gouge and allowed to equilibrate at room temperature for ~4 d. This process produced a solution that was in equilibrium with $CaCO_3$, at room temperature, prior to our experiments. Chemical equilibrium conditions for a $CaCO_3$–H_20–CO_2 system is reached within 48 hr under conditions of room temperature (Sjoberg & Rickard 1984). We choose to saturate our experimental samples with the $CaCO_3$ solution as previous work has shown that pore fluid chemistry has a significant impact on the rates of calcite solution/precipitation (Zhang & Spiers 2005) and the rate of frictional strengthening in general (Renard *et al.* 2012). Our choice of saturating fluid was used to minimize changes in pore fluid chemistry during our experiments and to better reflect the composition of pore fluid surrounding carbonate-hosted faults at depth.

We performed our experiments (Table 1) in the BRAVA apparatus hosted in the HPHT Laboratory at INGV, Rome, Italy (Fig. 1a; Collettini *et al.* 2014). Calcite gouge was sheared in a double-direct shear configuration (Fig. 1b) at normal stresses from 1 to 100 MPa. In our experiments, two initially 5-mm-thick gouge layers are sandwiched between three steel forcing blocks (Fig. 1b). The two side blocks are held stationary, and the centre forcing block is driven downward causing shear to occur within the gouge layers. Normal stress is applied by the horizontal piston in load-feedback control mode and shear displacement accomplished by the vertical piston in displacement-feedback control. Forces are measured with stainless steel load cells (± 0.03 kN) and displacements are measured with LVDT's ($\pm 0.1\ \mu m$) attached to each piston. All experimental data were recorded at 10 kHz and then down sampled to 1–1000 Hz based on the shearing velocity

After construction and placement of the sample assembly into BRAVA (Fig. 1), a normal stress of 1 MPa was applied and the $CaCO_3$ solution was added to a flexible, plastic membrane surrounding the sample. As sample preparation occurred under room humidity conditions, all samples were allowed to saturate for 30 min at low normal stress (~1 MPa). Following saturation and the equilibration of layer thickness, normal stress was increased to the target value, and layer thickness was again monitored until a quasi-steady-state of mechanical compaction was obtained.

We then performed two distinct types of experiments, slide-hold-slide (SHS) experiments designed to investigate static frictional strengthening, and velocity-stepping experiments to investigate the

Table 1. Experimental data.

Normal stress (MPa)	Exp #(SHS, VS)	μ_{ss}	SHS velocity (μm s^{-1})	β (s^{-1})	β_c (s^{-1})	(a–b) range
1.0	i143	0.62	1.0	0.041	0.059	–
1.0	i096, i138	0.62	10	0.038	0.063	–0.002 to 0.003
1.0	i144	0.64	100	0.038	0.086	–
1.0	i146	0.65	1000	0.030	0.082	–
2.5	i042, i147	0.68	10	0.038	0.063	–0.001 to 0.006
	i095	0.63	0.3	0.033	0.042	–
	i151	0.61	0.5	0.035	0.047	–
	i045	0.63	1.0	0.041	0.042	–
	i086	0.65	3.0	0.039	0.043	–
5.0	i040, i258	0.67	10	0.036	0.056	–0.001 to 0.003
	i329, –	0.66	10	0.037	0.054	
	i088	0.65	30	0.032	0.058	–
	i046	0.68	100	0.033	0.066	–
	i087	0.65	300	0.031	0.069	–
	i085	0.66	1000	0.029	0.068	–
	i089	0.64	1300	0.029	0.072	–
	i098	0.63	3000	0031	0.073	–
10	i043, i141	0.67	10	0.018	0.048	0.001 to 0.005
	i047, –	0.66		0.020	0.044	
20	i093, i148	0.66	10	0.012	0.035	–0.001 to 0.011
50	i131	0.55	1.0	0.004	0.026	–
50	i097, i139	0.63	10	0.011	0.031	0.001 to 0.016
50	i142	0.63	100	0.014	0.037	–
50	i145	0.62	1000	0.017	0.045	–
100	i116, i140	0.62	10	0.008	0.026	–0.005 to 0.013

velocity dependence of friction. Each experiment began with a 7.5 mm shear run to develop a steady-state fabric within the gouge (Fig. 1c). In SHS experiments, the shear run-in was performed at the desired SHS shearing velocity, 0.3–3000 μm s^{-1}, whereas for the velocity step experiments, the shear run-in was performed at 10 μm s^{-1}. This was done to ensure that samples collected for microstructural analysis, exclusively from SHS tests, experienced only one shear velocity. The steady-state coefficient of friction (μ_{ss}) was measured during the run-in phase and calculated as the ratio of shear stress to normal stress assuming no cohesion. In SHS experiments, load point velocity is changed from the chosen shearing velocity to 0 μm s^{-1} for a given hold time, and then back to same shearing velocity (Figs 2a and b). We performed holds of 1, 3, 10, 30, 100, 300, 1000 and 3000 s with 0.65 mm displacement after each hold. The amounts of frictional strengthening ($\Delta\mu$) and creep relaxation ($\Delta\mu_c$) are determined for each hold (Fig. 2b). We then determine the rates of frictional strengthening (β) and creep relaxation (β_c):

$$\beta = \Delta\mu/\log_{10} t_h, \tag{1}$$

$$\beta_c = \Delta\mu_c/\log_{10} t_h, \tag{2}$$

where t_h is the hold time (Fig. 2c). The parameter β provides an estimate of the rate of increase in static frictional strength. The recovery of frictional strength is one requirement for repeated earthquakes on the same fault (Brace & Byerlee 1966; Dieterich 1978). Creep relaxation during a hold is thought be related to earthquake afterslip (Marone *et al.* 1991) and constitutive friction properties (Beeler *et al.* 1994; Marone 1998a). Creep relaxation of the sample occurs due to elastic relaxation of the experimental load frame and the creeping of the experimental fault (Fig. 2c) during the hold period. Some research has shown that a SHS test can induce transient and/or semi-permanent changes in sliding friction (e.g. Karner *et al.* 1997; Muhuri *et al.* 2003; Chen *et al.* 2015). It is suggested that this occurs when the processes that occur during frictional aging disrupt shear localization (e.g. Sleep *et al.* 2000). We did not observe such transient or permanent increases in sliding friction during our experiments and thus do not explore this further.

In velocity stepping experiments, following the shear run-in (Figs 2d–f), the load point velocity is increased in the following sequence, 0.1–0.3–1–3–10–30–100–300–1000 μm s^{-1}, with 0.70 mm displacement at each step. The velocity dependence of friction is determined in the rate- and state-friction framework (Dieterich 1979; Ruina 1983) by modelling (e.g. Reinen & Weeks 1993; Blanpied *et al.* 1998) the data to determine the friction rate parameter (a–b):

$$(a-b) = \Delta\mu_{ss}/\Delta \ln V, \tag{3}$$

where μ_{ss} is the steady state friction coefficient and V is sliding velocity (Fig. 2e; e.g. Marone 1998a). We determined values of a–b and other constitutive parameters by fitting our data using an inverse modelling technique (e.g. Blanpied *et al.* 1998) with Dieterich's (1979) time-dependent friction law with two state variables:

$$\mu = \mu_0 + a\ln(V/V_0) + b_1\ln(V_0\theta_1/D_{c1}) + b_2\ln(V_0\theta_2/D_{c2}) \tag{4}$$

$$\mathrm{d}\theta_i/\mathrm{d}t = 1 - (V\theta_i/D_{ci}),\ (i = 1,\ 2), \tag{5}$$

where a, b_1 and b_2 are empirically derived constants (dimensionless), θ_1 and θ_2 are state variables with units of time, and D_{c1} and D_{c2} are critical slip distances (e.g. Marone 1998a). Most of our data are fit well with a one state variable friction law ($b_2 = \theta_2 = 0$), making the last term of eq. (4) unnecessary. However, some of our data required two state variables. A two state variable friction law was used when fitting the raw data with a one state variable friction law could not be done adequately. This is generally evident from the existence of friction evolution over both short- and long-distances. In these cases the inversion did not converge within a specified overall error/misfit or if it converged, produced a poor fit to the raw data on the basis of visual examination. We report values of (a–b), a, and b, and define $b = b_1 + b_2$ to compare one and two state variable cases. Positive values of (a–b), termed velocity strengthening, are

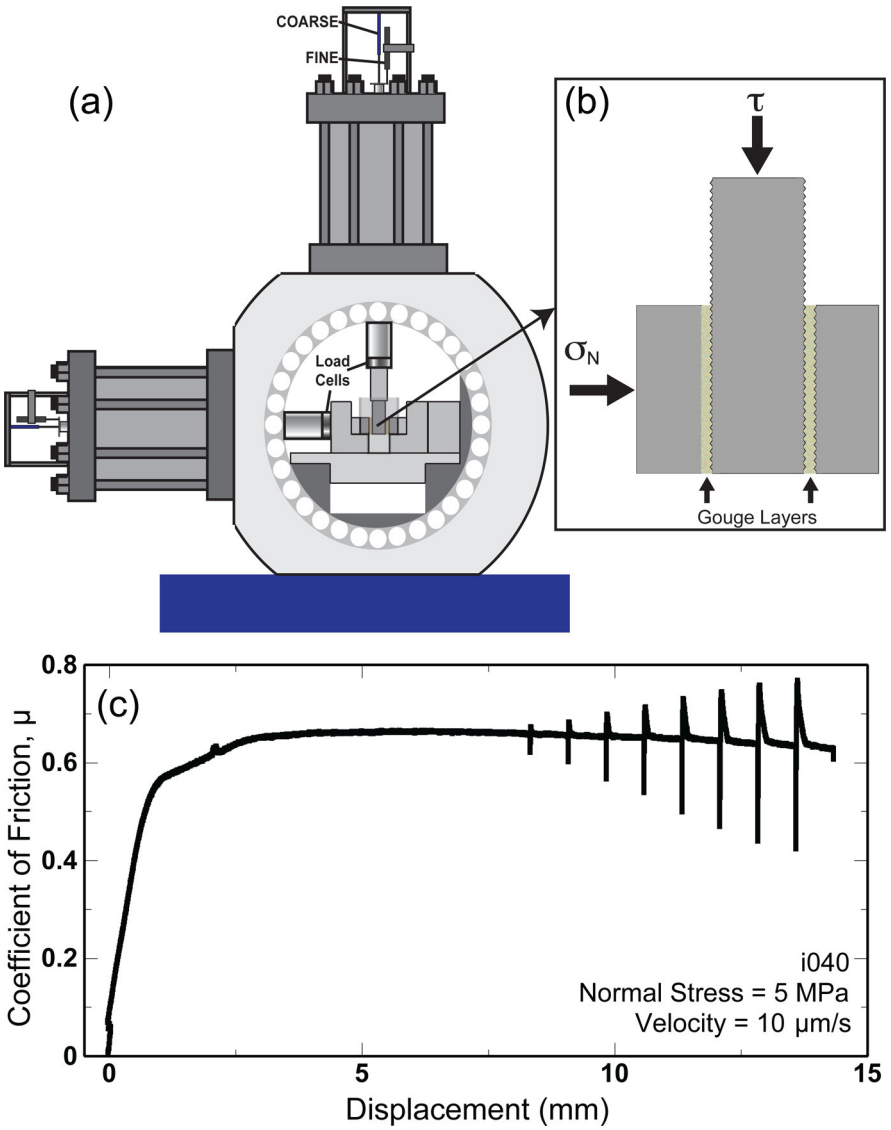

Figure 1. (a) Schematic of the BRAVA experimental apparatus in a double-direct shear configuration. (b) Details of the grooved steel forcing blocks used in this study. (c) Representative raw data for a slide-hold-side (SHS) experiment.

associated with stable sliding and inhibit rupture nucleation. Negative values, termed velocity weakening are a prerequisite for unstable slip and earthquake nucleation (e.g. Gu *et al.* 1984).

3 RESULTS

3.1 Mechanical behaviour

3.1.1 Frictional strength

We find that the steady-state frictional strength of saturated calcite fault gouge ranges between 0.55 and 0.68 over a range of normal stresses and velocities (Fig. 3; Table 1). At a shearing rate of 10 μm s^{-1}, we find a coefficient of friction of, μ = 0.63 (Fig. 3a), consistent with previous research on pure calcite gouge (Verberne *et al.* 2014b, 2015; Chen *et al.* 2015; Giorgetti *et al.* 2015) and other calcite-rich gouges (e.g. Weeks & Tullis 1985; Verberne *et al.* 2010; Scuderi *et al.* 2013; Carpenter *et al.* 2014; Chen et al 2015) under similar experimental conditions of normal stress, temperature and saturation. At a normal stress of 5 MPa and velocities ranging from 0.3 to 3000 μm s^{-1}, we observe what appears to be an increase in steady-state frictional strength until a velocity of 30–100 μm s^{-1} followed by a decrease (Fig. 3b). The observed changes in frictional strength with sliding velocity are small, but consistent over our velocity range and consistent with the idea of an intermediate velocity friction barrier (e.g. Di Toro *et al.* 2011, and references therein).

3.1.2 Friction strengthening and creep relaxation

The rates of frictional strengthening and creep relaxation for saturated calcite depend on both normal stress and sliding velocity (Fig. 4; Table 1). We observe that these rates are highest at our lowest normal stress. At a shearing rate of 10 μm s^{-1}, we observe a significant decrease in the rates of frictional strengthening and creep relaxation between normal stresses of 1 and 20 MPa (Fig. 4a). The rates then exhibit a more gradual decrease with further increases in normal stress to 100 MPa. At 10 μm s^{-1} velocity, we observe a consistent difference between the rates of frictional strengthening and creep relaxation that does not change with changes in

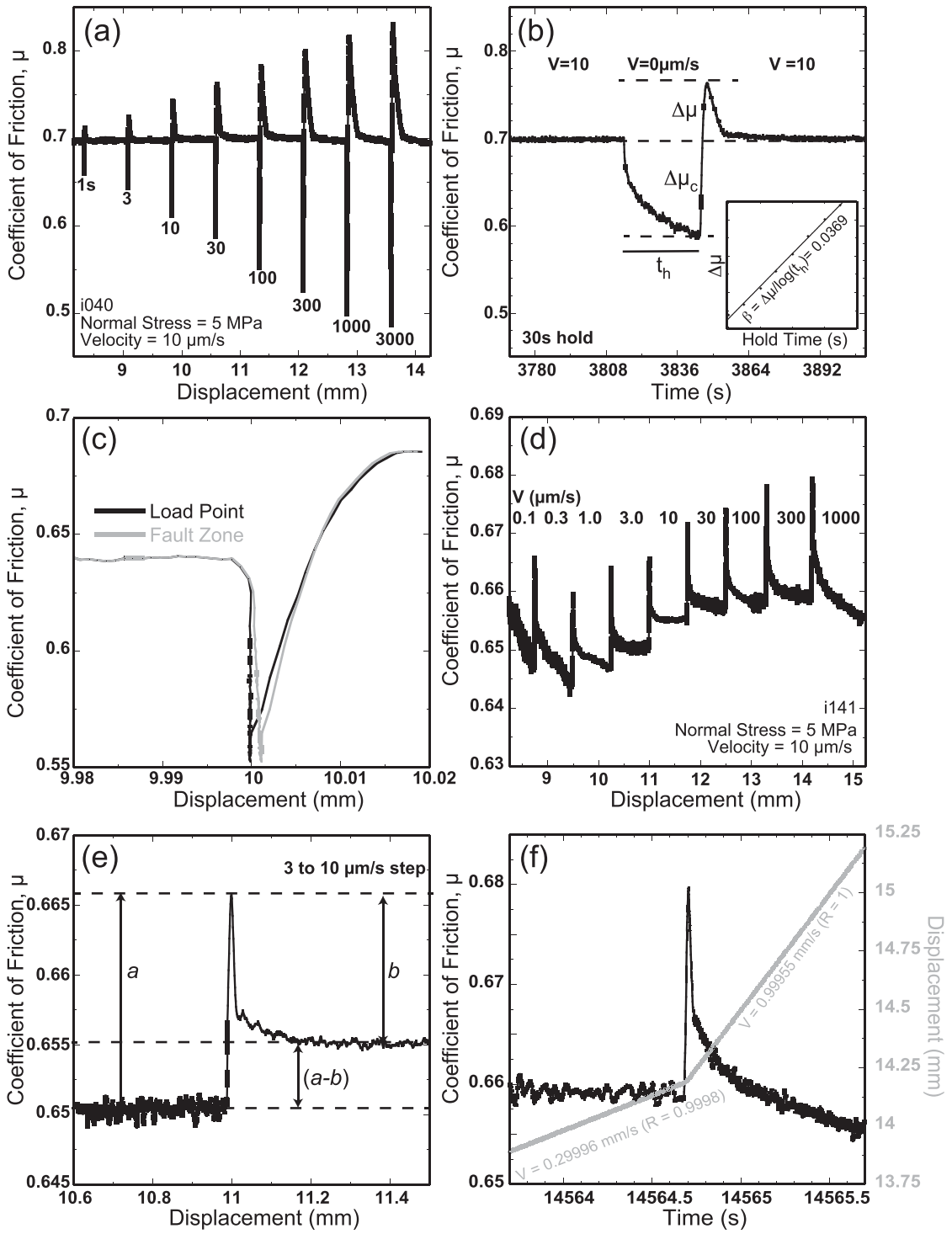

Figure 2. (a) Details of the SHS procedure used in this study. (b) The measured healing parameters. Inset: Example determination of frictional strengthening rate. (c) Data for a 10 s hold showing that the load point maintains a constant position while the sample creeps forward. (d) Details of the velocity-stepping procedure used in this study. (e) Schematic illustration showing the friction constitutive parameters a, b and a–b for a velocity strengthening rate step. (f) Friction and displacement shown against time for a 300–1000 μm s^{-1} velocity step.

normal stress (Fig. 4a). Our measured rates of frictional healing are consistent with experiments performed under similar conditions on calcite-rich gouge (Carpenter *et al.* 2014; Tesei *et al.* 2014; Chen *et al.* 2015; Giorgetti *et al.* 2015), which in some cases have shown decreases in the amount of frictional strengthening with increasing normal stress (Tesei *et al.* 2014). Coefficient of determination (R^2) values for our determined strengthening and creep relaxation rates are reported in Table S1.

We observe a complex dependence of the rates of frictional strengthening and creep relaxation on sliding velocity. At a normal stress of 5 MPa and a velocity of 1 μm s^{-1}, the rates are nearly equal, and then diverge as velocity is increased to ∼1000 μm s^{-1},

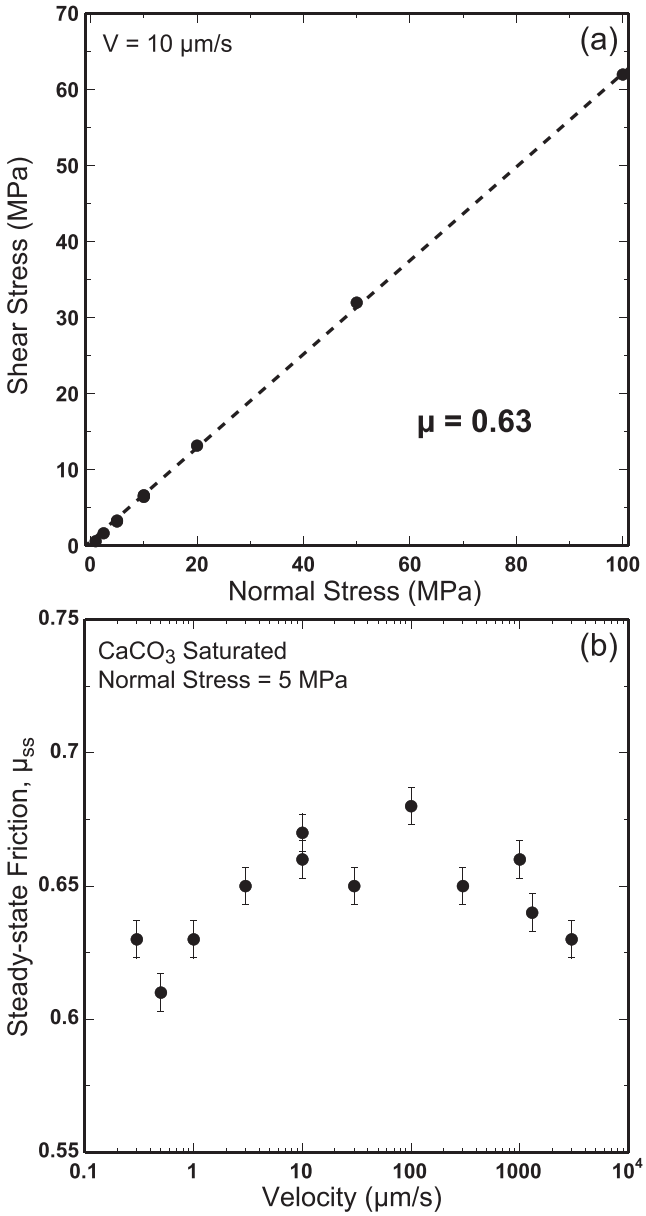

Figure 3. (a) Coulomb–Mohr failure envelope for the calcite gouge used in our study. (b) Steady-state friction coefficient plotted against loading velocity at a normal stress of 5 MPa.

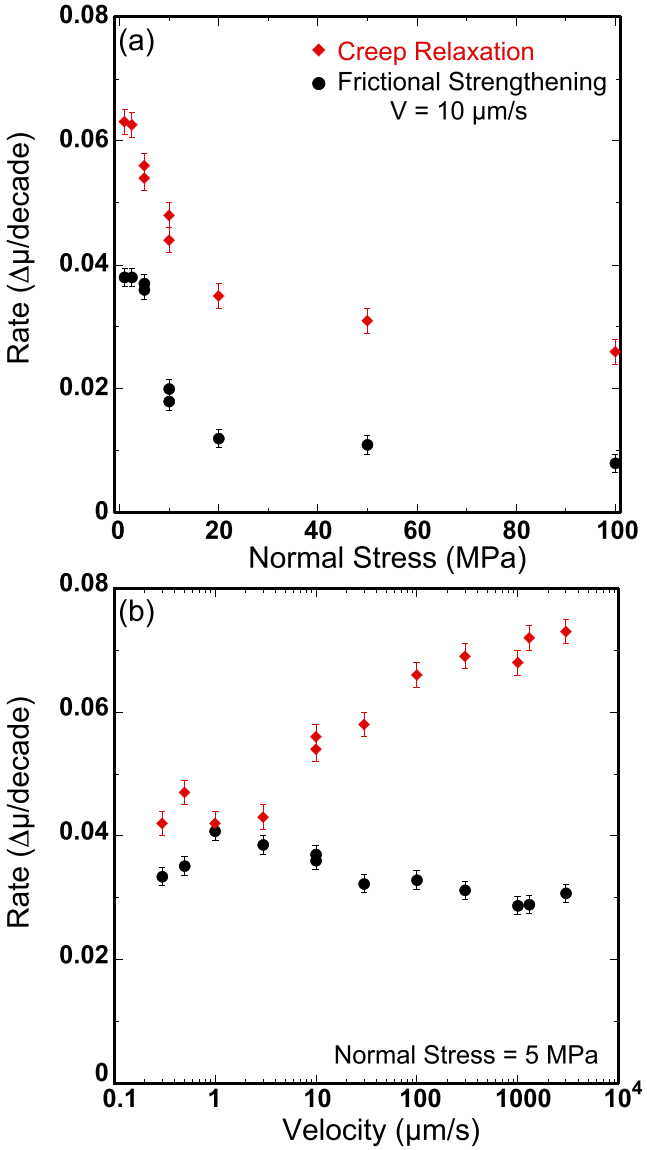

Figure 4. Frictional strengthening and creep relaxation rates shown against normal stress (a) and velocity (b). Note the rapid decrease in both the rates of frictional strengthening and creep relaxation between 1 and 20 MPa normal stress. Also note the complex dependence of each rate on velocity.

after which they appear to remain constant (Fig. 4b). With decreasing velocity, below 1 μm s^{-1}, we observe that the rate of creep relaxation remains relatively constant, while the rate of frictional strengthening decreases. Our observations are consistent with observations of decreased frictional strengthening rates in calcite gouge when the shearing rate is decreased from 10 to 1 μm s^{-1} (Chen *et al.* 2015). However, our work is not consistent with previous experiments, on quartz gouge, which have shown the rates of frictional strengthening and creep relaxation to be independent of shearing rate (e.g. Marone 1998b).

3.1.3 Velocity dependence of friction

We also observe complex relationships between the velocity dependence of friction and normal stress and sliding velocity (Fig. 5; Table 1). At low normal stresses, ≤20 MPa, we observe velocity neutral to slight velocity strengthening friction behaviour, with a relatively narrow range for our friction rate parameter (*a–b*) data (Fig. 5a). As normal stress is increased to 100 MPa, we observe an increasing range in (*a–b*) and mostly velocity strengthening behaviour (Fig. 5a). When shown against velocity, we observe two distinct types of behaviour for frictional stability. At normal stresses ≤20 MPa, we observe velocity neutral to velocity strengthening behaviour over the entire velocity range (Fig. 5b). However, once normal stress exceeds 20 MPa, We observe an increasing, strongly velocity strengthening behaviour to velocities of 3–10 μm s^{-1}. Subsequently, we observe a decrease in the value of (*a–b*) that frequently results in velocity weakening friction behaviour at a velocity of 1000 μm s^{-1} (Fig. 5b). Overall, our data for the velocity dependence of friction, (*a–b*), are consistent with previous data for calcite-rich gouges under similar experimental conditions (Verberne *et al.* 2010,

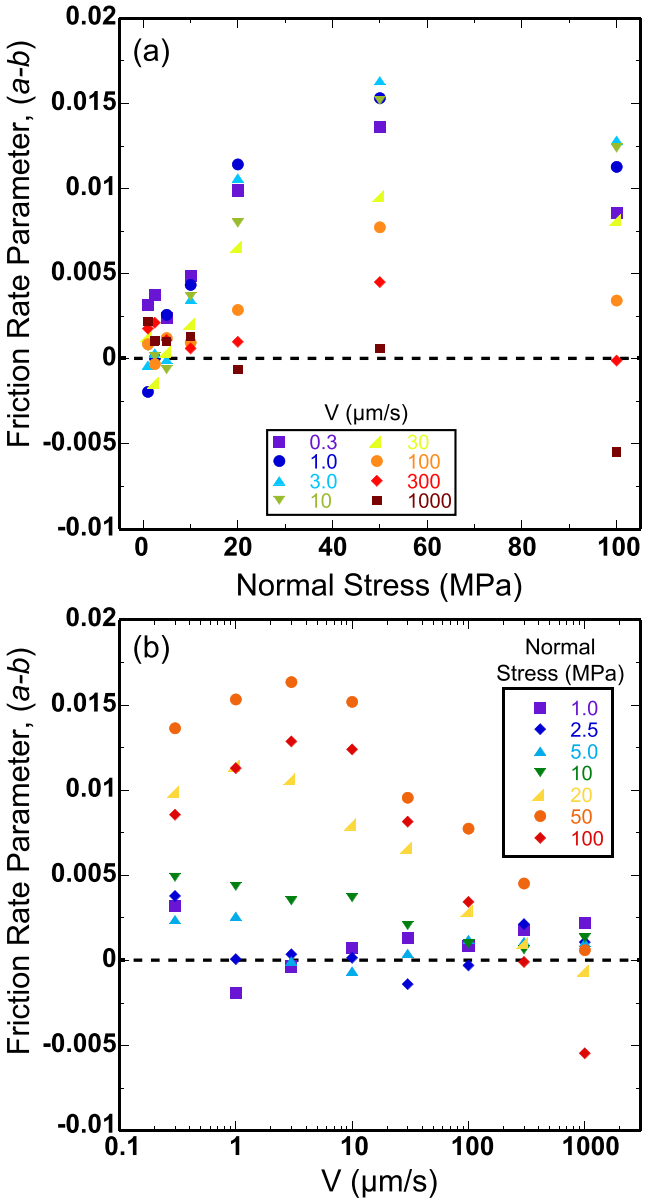

Figure 5. Friction rate parameter, *a*–*b*, shown as functions of normal stress (a) and velocity (b). At low normal stresses and velocities, calcite shows primarily velocity-neutral friction behaviour. At higher normal stress, the behaviour evolves from strong velocity strengthening behaviour at low velocities to velocity-neutral behaviour at high velocities.

Scuderi *et al.* 2013; 2014b; Carpenter *et al.* 2014; Tesei *et al.* 2014, 2015; Chen *et al.* 2015; Giorgetti *et al.* 2015).

We further consider the roles of normal stress and velocity on frictional stability by examining the evolution of the friction rate parameters *a* and *b* independently (Fig. 6). We observe decreases in both *a* and *b* with increasing normal stress. We observe the largest changes, with respect to increasing normal stress, at the lowest velocities studied. At 100 MPa, *a* approaches 0 at velocities <3 μm s^{-1}, whereas *b* becomes negative over a similar velocity range (Figs 6a and b). The range of values is the smallest at low normal stresses and increases with increasing normal stress. If we specifically compare data at 1 and 50 MPa, low and high normal stress, we observe that at 1 MPa, *a* and *b* are larger in magnitude, than at 50 MPa, and in general remain relatively constant with increasing velocity (Figs 6c and d). At 50 MPa, *a* shows a small but consistent trend of increasing with velocity. *b* begins negative at slow velocities, and then increases at a faster rate than *a* after a velocity of 10 μm s^{-1}. The transition of *a* towards 0 and *b* to negative values, at low velocities, with increasing normal stress is consistent with a transition in deformation from brittle to ductile that has been previously observed in direct shear experiments (Shimamoto 1986; Noda & Shimamoto 2010). We explore this further in the discussion section.

3.2 Microstructural analysis

The starting material (Fig. S1), pulverized Carrara marble sieved to <150 μm, is characterized by an heterogeneous grain size distribution with a high concentration of fine material: 50 per cent of the volume is characterized by a grain size <16 μm. At low normal stresses (<10 MPa) microstructural observations confirm the heterogeneous grain size, with angular grains isotropically distributed in a finer matrix (Figs 7a and b). The finer matrix is made of grains with irregular boundaries where nanograins concentrate (Fig. 7c). Comparison with the microstructure of the starting material indicates that these nanograins formed during the experiments and are not the result of the milling process. Furthermore, the poorly cemented fine-ultrafine matrix seems to link different portions of the matrix (Fig. 7c). Discontinuous geometrical features characterized by irregular boundaries, and not affected by localized grain size reduction, are parallel or at low angles with respect to the fault boundaries (Figs 7a and b). At high normal stresses ($\geq$50 MPa) the angular grains distributed in the finer matrix are affected by pervasive intragranular fractures. In some portions of the fault, we observe grain size reduction along R1 shear planes (e.g. Logan *et al.* 1979; Logan & Rauenzahn 1987) that are oriented with en-echelon geometry and characterized by straight boundaries (Figs 7d and e). In other portions we observe features with zig-zag boundaries, subhorizontal or antithetic to R1 shear planes and not characterized by grain size reduction (Fig. 7d). Additionally at higher stresses, nanograins, 10–100 nm in size, are present and form a continuous and interconnected network all around relatively larger calcite crystals (Fig. 7f). This observation is similar to that made by Chen *et al.* (2015) at the same normal stress, but higher temperature (their fig. 7g). Microstructural investigations on experimental faults at 5 MPa and at different sliding velocities (i.e. 0.3 μm s^{-1} in i095 versus 3000 μm s^{-1} in i098) indicate that the difference in sliding velocity does not influence the microstructure evolution (Fig. S2), at least to the same extent as normal stress.

Further analysis of the experimental sample from the experiment performed at 50 MPa normal stress was performed on via an optical microscope (Fig. 8). At this normal stress, in addition to the R1 shears visible under the SEM, we also observe deformation along B, and Y shear planes (e.g. Logan *et al.* 1979) where there is significant grain size reduction. Some portions of the experimental fault are not affected by grain size reduction: here the calcite crystals are up to 150 μm in dimension and show an intense twinning typical of the starting Carrara marble. The most striking feature is that along B, Y and R1 shear planes, we do not observe the typical grain size reduction associated with localization, but rather an anastomosing network of low-birefringence material pervading all the zones affected by grain size reduction and shearing (Fig. 8b). Within this anastomosing network, surviving calcite crystals show fading grain boundaries and in some cases, their border abruptly terminates in the low-birefringence material (Figs 8c and d).

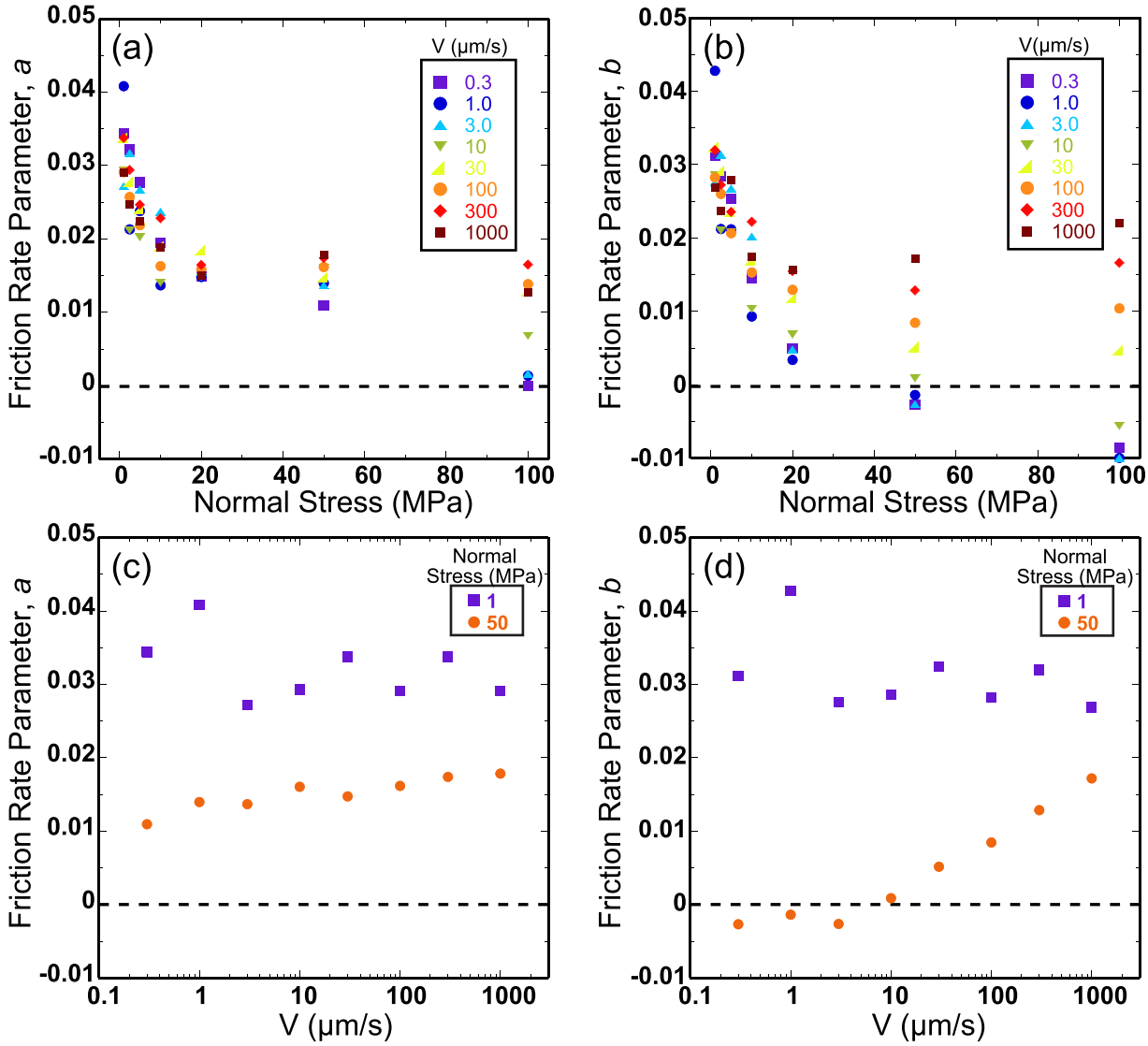

Figure 6. Friction rate parameters a and b shown as a function of normal stress (a, b) and velocity (c, d). Note that in (c, d) we only show data for normal stresses of 1 and 50 MPa.

4 DISCUSSION

4.1 Microphysical behaviour

Previous studies have shown that the deformation of calcite at shallow crustal conditions and velocities, comparable to those experienced during the nucleation of earthquakes, occurs by a variety of deformation mechanisms (e.g. Fredrich *et al.* 1989; Schubnel *et al.* 2006; Verberne *et al.* 2013, 2014b, 2015; Chen *et al.* 2015). These studies have shown that at relatively low temperatures and normal stresses ($T < 100$ °C and $\sigma_n' < 100$ MPa), processes such as pressure solution, interacrystalline plasticity, superplastic flow of nanogranular calcite, and frictional sliding are all active. Understanding the interplay and competition between these mechanisms and how they influence fault behaviour and earthquake nucleation is a critical goal of these studies.

Our mechanical results indicate that we observed the brittle/semi-brittle (Shimamoto 1986; Evans *et al.* 1990; Noda & Shimamoto 2010) transition for calcite gouge in our experiments. Furthermore, our data show how the transition from brittle to semi-brittle behaviour, and the presence of related deformation mechanisms, influences the frictional behaviour of calcite fault gouge. This transition in deformation, from brittle to semi-brittle is first indicated by the evolution of the friction rate parameter, b (Fig. 6d). This parameter, often termed the evolution effect, is thought to represent the evolution of contact area upon a velocity perturbation (e.g. Marone 1998a). At low normal stress, we observe relatively constant and positive values of b, which suggests a dominantly brittle mode of behaviour over the entire velocity range (0.1–1000 μm s^{-1}). At higher normal stress, we observe a transition from negative values of b, to positive values of b with increasing velocity (Fig. 7d). Our observations of negative b in calcite gouge at room temperature are consistent with other studies that have shown similar behaviour under comparable conditions of temperature and velocity (Verberne *et al.* 2014b; Chen *et al.* 2015). Additionally, both the negative values for b and the near zero value for β are also consistent with the saturation of contact area, which would be expected to occur under conditions of ductile deformation. To better characterize and illustrate this behaviour and how it evolves with normal stress and velocity, we present additional data and interpretation (Fig. 9). The transition from brittle to semi-brittle deformation is controlled by

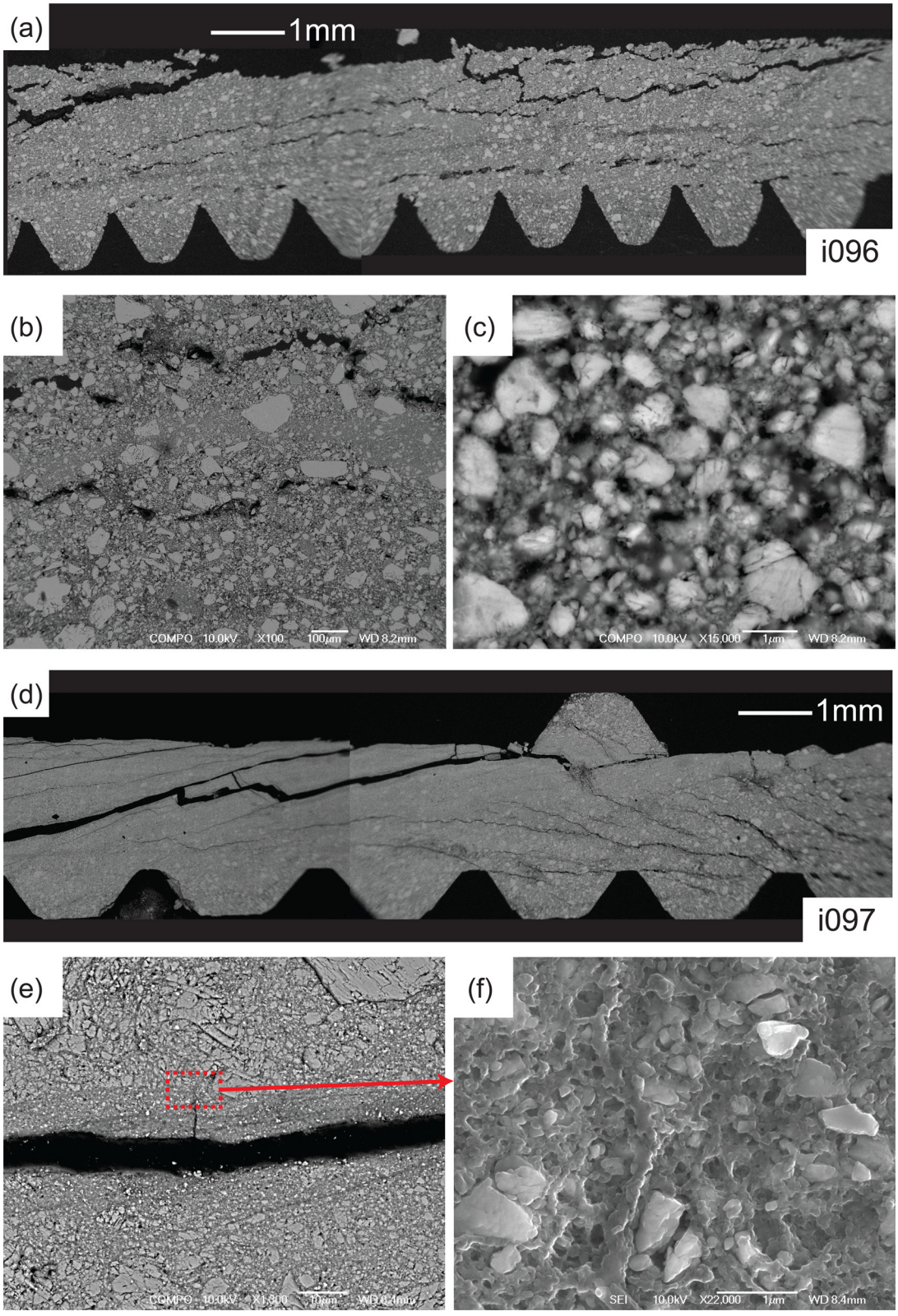

Figure 7. Microstructures of experimentally deformed gouges from experiments at 1 (a–c) and 50 (d–f) MPa normal stress. See text for description.

both normal stress and velocity. At velocities $\geq$1 μm s^{-1}, we observe a linear failure envelope over our entire velocity range, with μ = ~0.64 (Fig. 9a). Pressure dependent strength is consistent with frictional (i.e. brittle) processes. At velocities $\leq$1 μm s^{-1}, we observe a linear failure envelope to a normal stress of 20 MPa, that then begins to deviate at higher stresses, consistent with an eventual transition to pressure independent strength (Fig. 9a). This is consistent with the evolution of halite gouge to ductile behaviour under similar experimental conditions (Shimamoto 1986). The transition to semi-brittle behaviour is also observed in slide-hold-slide (Fig. 9b) and

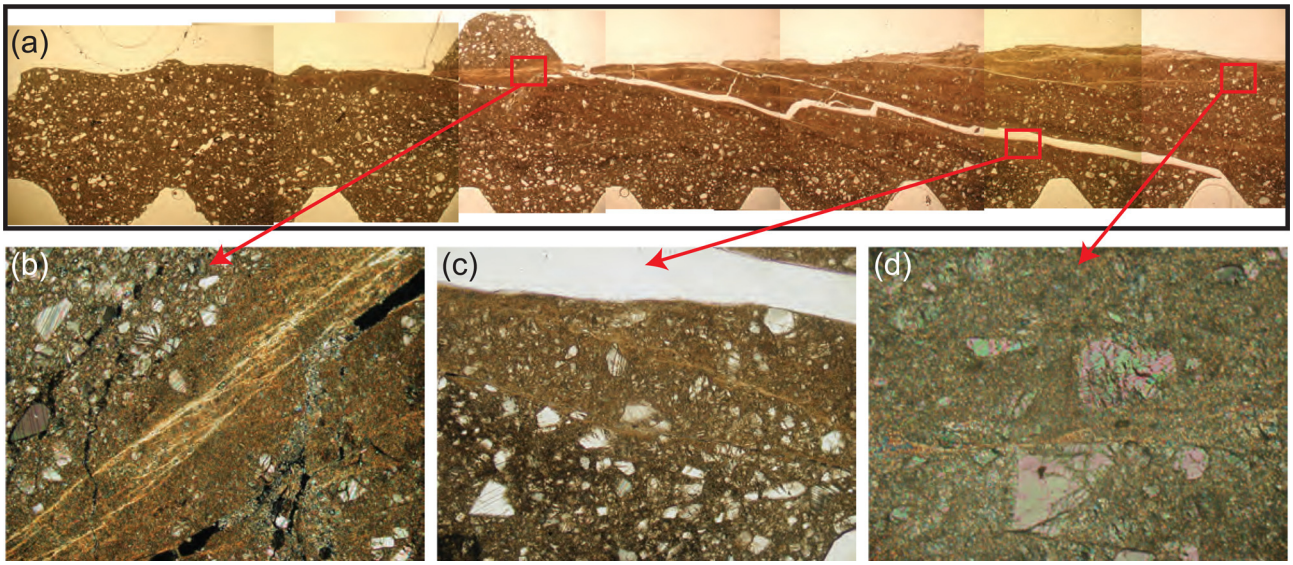

Figure 8. Optical micrographs of the experimental gouge from an experiment at 50 MPa normal stress. See text for description.

velocity step experiments (Fig. 9c). In SHS tests performed at normal stresses of 1 and 50 MPa and a background-loading rate of 1 μm s^{-1}, we observe typical brittle behaviour at 1 MPa and semi-brittle behaviour at 50 MPa. This is evidenced by the relatively stiffer reload and sharp, large peak in friction at 1 MPa compared to the relatively less stiff reload and broader, small peak at 50 MPa (Fig. 9b). In velocity step experiments, we observe brittle behaviour at low normal stress, over the entire velocity range and a transition from semi-brittle to brittle behaviour, with increasing sliding velocity, at high normal stress (Fig. 9c). This is consistent with the transition in frictional response upon a velocity step observed by Noda and Shimamoto (2010) where under ductile conditions they observed a monotonic increase, values of the friction rate parameter $b \leq 0$, that transitioned to peak decay and frequent velocity-weakening behaviour under brittle conditions.

4.2 Microstructure interpretation and the transition from brittle to semi-brittle deformation

Our microstructural analysis shows the presence of both brittle deformation, characterized by granular fracture, grain size reduction and localization (Figs 7d,e, 8 and 9d), and semi-brittle deformation with dissolution and precipitation (Figs 7e, 8, and 9d), granular fracture and folding. In particular, calcite crystals with fading grain boundaries that terminate into the low-birefringence anastomosing material suggest dissolution of calcite crystals favoured along the twinning planes that represent planes of structural weakness. Microscopic analyses shows that the low-birefringence material consists of newly formed (unstrained crystals) nanograins (100 nm) that for their small thickness develop a low-birefringence. Therefore in the areas of shearing, that is B, Y and R planes, we propose that grain-size reduction promoted fluid-assisted solution transfer processes with the precipitation of nanogranular material forming an anastomosing network. Similar nanogranular material has been observed by Verberne *et al.* (2013, 2015) in samples from experiments performed under the same boundary conditions, 50 MPa normal stress and room temperature: here the microstructure results from diffusion mass transfer processes and crystal plastic deformation (Verberne *et al.* 2013, 2015).

Our mechanical and microstructural analysis, combined with previous work, supports our interpretation of a change from semi-brittle behaviour at low velocities to brittle behaviour at higher velocities. Our work is consistent with previous studies that have mapped this transition in Carrara Marble under similar conditions of temperature normal stress, and strain rate in different experimental configurations, that is triaxial experiments on cylindrical cores (e.g. Fredrich *et al.* 1989; Brantut *et al.* 2014). Fredrich *et al.* (1989) observed this transition at room temperature and between confining pressures of 25 and 75 MPa, depending on grain size. Furthermore, they observed a transition from shear localization at low confining pressures to distributed deformation at higher confining pressures (Fredrich *et al.* 1989). We note that this work was not preformed under saturated conditions. Brantut *et al.* (2014) also observed this transition in water-saturated limestone samples at strain rates of 10^{-5} s^{-1}. We note that our determined shear strain rates at our lowest velocities are on the order of 10^{-5}–10^{-4} s^{-1}, entirely consistent with previous work that has shown ductile behaviour in calcite-rich rocks at room temperature.

At low velocities and high stresses, both plastic deformation of calcite grains (Fig. 9d; e.g. Schubnel *et al.* 2006) and sliding deformation accommodated by solution transfer processes (Figs 8b–d; e.g. Rutter & Manprice 1979) could result in the observed semi-brittle behaviour (Shimamoto 1986; Noda & Shimamoto 2010). The observed behaviour in b, as well the rapid static strengthening and the numerous microstructural observations support the interpreted presence of solution transfer processes. The decrease in frictional strengthening with increased normal stress (Fig. 4a) is consistent with a diffusion controlled solution transfer process, as low porosity would result in the reduction of the available paths for fluid transport. The semi-brittle behaviour of calcite at conditions representative of the shallow crust would be expected to exert influence over the mechanical behaviour of the fault. While not the explicit goal of this study, we recognize that our work can inform past and ongoing work performed to better understand the microphysical foundations of rate- and state-friction law and develop mechanism based inputs (e.g. Chester & Higgs 1992; Sleep *et al.* 2000; Nakatani 2001; Niemeijer & Spiers 2007; Putelat *et al.* 2011; Verberne *et al.* 2015).

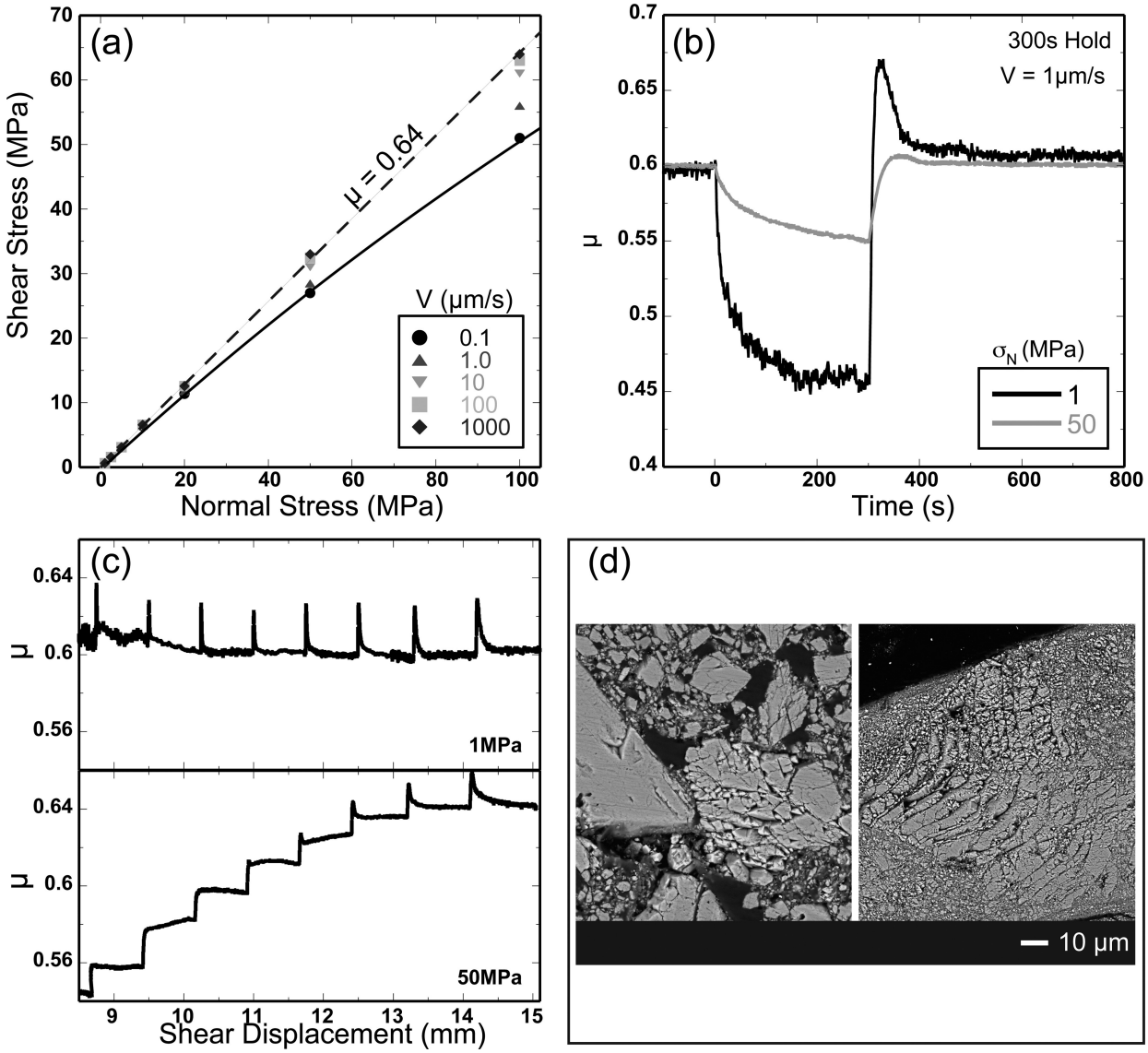

Figure 9. Data and analysis showing the transition from brittle to semi-brittle behaviour. (a) Coulomb–Mohr failure envelope for different shearing velocities. Dashed line indicates linear fit to data at $V = 1000$ μm s^{-1}. Solid line is a fiducial line through data at $V = 0.1$ μm s^{-1}. Actual values of shear stress at high stress (≥50 MPa) and low velocity (<1 μm s^{-1}) are likely slightly lower than reported values as steady-state was not achieved in all cases. (b) Raw data for SHS experiments at 1 and 50 MPa normal stress performed at a velocity of 1 μm s^{-1}. Note nearly 0 strengthening and more compliant reload. (c) Raw data for velocity steps at 1, top and 50, bottom, MPa normal stress. At low normal stress, brittle behaviour is observed over the entire velocity range. At high normal stress, a transition is observed from semi-brittle behaviour at low velocity, to brittle behaviour at high velocity. Velocity sequence is the same as shown in Fig. 2(d). (d) SEM images showing evidence of brittle, left, and semi-brittle, right, behaviour.

4.3 Implications for fault behaviour

Several well-documented, carbonate-hosted, seismic sequences, e.g. Umbria-Marche 1997–1998 (Mirabella *et al.* 2008) and L'Aquila 2009 (Valoroso *et al.* 2014) show that a significant number of aftershocks nucleate at very shallow crustal levels, up to 500 m of depth. In addition, the Varoni borehole, located in the northern portion of the L'Aquila seismic sequence shows temperatures of 46 and 67 °C at crustal depths of 3.70 and 5.70 km, respectively (ViDEPI project; http://unmig.sviluppoeconomico.gov.it/videpi/videpi.asp). Together, these data indicate that our laboratory measurements, conducted at room temperature, can be used to further our understanding of the seismicity occurring in carbonates at shallow crustal levels. For the seismicity occurring at greater depths, the transition from velocity-strengthening to velocity-weakening frictional behaviour at temperatures greater than 100 °C, observed in some experiments on calcite, can provide additional understanding (e.g. Verberne *et al.* 2015). In general our data show a velocity neutral to strengthening behaviour, which would favor stable sliding and fault creep (Fig. 5). However, at low normal stresses we document dominantly velocity-neutral behaviour and at higher normal stresses, we observe a transition to velocity-weakening behaviour with increasing sliding velocity (Fig. 5). In addition, it is worth noting that accelerated post-seismic slip can drive aftershock activity in fault portions that are velocity neutral or slightly velocity strengthening (Boatwright & Cocco 1996).

In areas of lower normal stress, either at shallow depths or due to high pore fluid pressure, we would expect enhanced post-seismic creep, due to high rates of creep relaxation (Fig. 4), which would be expected to drive aftershock activity. Such behaviour was observed

for the 2009 L'Aquila earthquake where the rupture is thought to have nucleated in an area of high-fluid pressure, and thus low normal stress (Lucente *et al.* 2010; Di Stefano *et al.* 2011; Malagnini *et al.* 2012). The rupture then propagated to the surface where significant aftershocks were observed to depths as shallow as 1 km (D'Agostino *et al.* 2012; Valoroso *et al.* 2014). At high normal stresses, strong velocity-strengthening friction behaviour, at low velocities, would initially resist rupture nucleation and propagation (Fig. 5b). This data could in part explain why rupture initially nucleated in an area of low normal stress propagated quickly to the surface, in the direction of decreasing normal stress (Cirella *et al.* 2009). The observation of delayed rupture along strike, at depth in an area of higher normal stress, is consistent with our data that shows rupture would be resisted initially, and then favoured as the velocity increased. We recognize that our results are not the only possible explanation. Other explanations for the observed behaviour could result from differences in fault structure (Di Stefano *et al.* 2011; Trippetta *et al.* 2013; Carpenter *et al.* 2014) and/or temperature effects on frictional properties (e.g. Verberne *et al.* 2015). The depth dependence and heterogeneity of frictional properties along faults have been widely cited to explain locations of rupture nucleation, directivity in rupture propagation, post-seismic slip, and aftershock activity (e.g. Tse & Rice 1986; Boatwright & Cocco 1996; Collettini *et al.* 2011; Carpenter *et al.* 2014; Niemeijer & Vissers 2014).

5 CONCLUSIONS

We have presented a comprehensive data set on the frictional behaviour of calcite at shallow crustal conditions. Our mechanical data, frictional strength, stability, and strengthening behaviour, are derived from room temperature experiments performed between 1 and 100 MPa normal stress and at velocities that range from tenths of $\mu m\ s^{-1}$ to thousands of $\mu m\ s^{-1}$. We have shown that the frictional strengthening and stability behaviour of calcite is strongly dependent on normal stress and shear velocity. We observed a strong dependence of the rates of frictional strengthening and creep relaxation on normal stress, with the rate of creep relaxation also showing a dependence on sliding velocity. Furthermore, we observe velocity neutral frictional behaviour at low normal stresses and all velocities where microstructural investigations show that deformation is accommodated via comminution and grain rotation/translation. At higher normal stress, we observe strong velocity strengthening behaviour at low sliding velocity, consistent with semi-brittle behaviour, followed by a transition to velocity weakening friction behaviour at the highest sliding velocity. This change in behaviour is accompanied with localized deformation along B, Y and R1 shear planes where grain-size reduction and fluid-assisted diffusion mass transfer play an important during deformation. All of our post-experimental samples indicate the presence of both frictional and solution transfer processes in our gouge layers.

The high rates of frictional strengthening and velocity neutral frictional behaviour of calcite gouge at low normal stresses, indicate that fault gouges where calcite plays a dominant mechanical role are likely to propagate ruptures that have started elsewhere and experience aftershock activity. Deeper in the crust, where normal stress exceeds 50 MPa, fault gouges dominated by calcite are likely to resist initial rupture nucleation at velocities below 30 $\mu m\ s^{-1}$. As the velocity continues to increase, rupture nucleation would accelerate due to the transition to velocity weakening frictional behaviour and possible dynamic weakening processes that would be expected to occur.

ACKNOWLEDGEMENTS

This research was carried out within the European Research Council, Starting Grant, GLASS (n° 259256). We thank Fabio Trippetta for important suggestions that helped to clarify some important aspects of this manuscript. We also thank Telemaco Tesei and Marco Scuderi for useful discussions and Giuseppe Di Stefano for technical assistance in the laboratory. We thank B. Kilgore, N. Brantut, and one anonymous reviewer for their constructive reviews, which significantly improved this manuscript.

REFERENCES

Beeler, N.M., Tullis, T.E. & Weeks, J.D., 1994. The role of time and displacement in the evolution effect in rock friction, *Geophys. Res. Lett.,* **21,** doi:10.1029/94GL01599.

Bernard, P. *et al.*, 1997. The Ms = 6.2, June 15, 1995 Aigion earthquake (Greece): evidence for low angle normal faulting in the Corinth rift, *J. Seismol.,* **1,** 131–150.

Blanpied, M.L., Marone, C.J., Lockner, D.A., Byerlee, J.D. & King, D.P., 1998. Quantitative measure of the variation in fault rheology due to fluid-rock interactions, *J. geophys. Res.,* **103,** 9691–9712.

Boatwright, J. & Cocco, M., 1996. Frictional constraints on crustal faulting, *J. geophys. Res.,* **101,** 13 895–13 909.

Bos, B. & Spiers, C.J., 2002. Fluid-assisted processes in gouge-bearing faults: insights from experiments on a rock analogue system, *Pure appl. Geophys.,* **159,** 2537–2566.

Brace, W.F. & Byerlee, J.D., 1966. Stick-slip as a mechanism for earthquakes, *Science,* **153,** 990–992.

Brantut, N., Heap, M.J., Baud, P. & Meredith, P.G., 2014. Mechanisms of time-dependent deformation in porous limestone, *J. geophys. Res.,* **119,** 5444–5463.

Burchfiel, B.C., Royden, L.H., van der Hilst, R.D. & Heger, B.H., 2008. A geological and geophysical context for the Wenchuan earthquake of 12 May 2008, Sichuan, People's Republic of China, *GSA Today,* **18,** doi:10.1130/GSATG18A.1.

Byerlee, J.D., 1968. Brittle-ductile transition in rocks, *J. geophys. Res.,* **73,** 4741–4750.

Carpenter, B.M., Scuderi, M.M., Collettini, C. & Marone, C., 2014. Frictional heterogeneities on carbonate-bearing normal faults: insights from the Monte Maggio Fault, Italy, *J. geophys. Res.,* **119,** 1–15.

Chen, J., Verberne, B.A. & Spiers, C.J., 2015. Interseismic re-strengthening and stabilization in carbonate faults by "non-Dieterich" healing under hydrothermal conditions, *Earth planet. Sci. Lett.,* **423,** 1–12.

Chester, F.M. & N. Higgs, G., 1992. Multimechanism friction model for ultrafine quartz gouge at hypocentral conditions, *J. geophys. Res.,* **97,** 1859–1870.

Cirella, A., Piatanesi, A., Cocco, M., Tinti, E., Scognamiglio, L., Michelini, A., Lomax, A. & Boschi, E., 2009. Rupture history of the 2009 L'Aquila (Italy) earthquake from non-linear joint inversion of strong motion and GPS data, *Geophys. Res. Lett.,* **36,** L19304, doi:10.1029/2009GL039795.

Collettini, C., Niemeijer, A.R., Viti, C., Smith, S.A.F. & Marone, C., 2011. Fault structure, frictional properties and mixed-mode fault slip behaviour, *Earth planet. Sci. Lett.,* **311,** 316–327.

Collettini, C. *et al.*, 2014. A novel and versatile apparatus for brittle rock reformation, *Int. J. Rock Mech. Min. Sci.,* **66,** 114–123.

D'Agostino, N., Cheloni, D., Fornaro, G., Giuliani, R. & Reale, D., 2012. Space-time distribution of afterslip following the 2009 L'Aquila earthquake, *J. geophys. Res.,* **117,** B02402, doi:10.1029/2011JB008523.

De Bresser, J.H.P., Evans, B. & Renner, J., 2002. On estimating the strength of calcite rocks under natural conditions, in *Deformation mechanisms, Rheology and Tectonics: Current Status and Future Perspectives*, pp. 309–329, eds De Meer, S., Drury, M.R., De Bresser, J.H.P. & Pennock, G.M., Geol. Soc., London, Spec. Publ., 200, Geological Society.

De Paola, N., Hirose, T., Mitchell, T., Toro, Di, G., Viti C. & Shimamoto, T., 2011. Fault lubrication and earthquake propagation in thermally unstable rocks, *Geology,* **39,** 35–38.

De Paola, N., Holdsworth, R.E., Viti, C., Collettini, C. & Bullock, R., 2015. Can grain size sensitive flow lubricate faults during the initial stages of earthquake propagation?, *Earth planet. Sci. Lett.,* **431,** 48–58.

Dieterich, J.H., 1978. Time-dependent friction and the mechanics of stick-slip, *Pure appl. Geophys.,* **116,** 790–805.

Dieterich, J.H., 1979. Modeling of rock friction: 1. Experimental results and constitutive equations, *J. geophys. Res.,* **84,** 2161–2168.

Di Stefano, R., Chiarabba, C., Chiaraluce, L., Cocco, M., De Gori, P., Piccinini, D. & Valoroso, L., 2011. Fault zone properties affecting the rupture evolution of the 2009 (MW 6.1) L'Aquila earthquake (central Italy): insights from seismic tomography, *Geophys. Res. Lett.,* **38,** L10310, doi:10.1029/2011GL047365.

Di Toro, G. *et al.*, 2011. Fault lubrication during earthquakes, *Nature,* **471,** doi:10.1038/nature09838.

Edmond, J.M. & Paterson, M.S., 1972. Volume changes during the deformation of rocks at high pressures, *Int. J. Rock Mech. Min. Sci*., **9,** 161–182.

Evans, B., Fredrich, J.T. & Wong, T.-F., 1990. The brittle-ductile transition in rocks: recent theoretical and experimental progress, in *The Brittle-Ductile Transition in Rocks—The Heard Volume*, pp. 1–20, eds Duba, A.G., Durham, W.D., Handin, J.W. & Wang, H.F., Geophys. Monogr., 56, AGU.

Fondriest, M., Smith, S.A.F., Candela, T., Nielsen, S.B., Mair, K. & Di Toro, G., 2013. Mirror like faults and power dissipation during earthquakes, *Geology,* **41,** 1175–1178.

Fredrich, J.T., Evans, B. & Wong, T.-F., 1989. Micromechanics of the brittle to plastic transition in Carrara marble, *J. geophys. Res.,* **94,** 4129–4145.

Giorgetti, C., Carpenter, B.M. & Collettini, C., 2015, Frictional behavior of talc-calcite mixtures, *J. geophys. Res.,* **120,** 6614–6633.

Govoni, A. *et al.*, 2014. The 2012 Emilia seismic sequence (Northern Italy): imaging the thrust fault system by accurate aftershock location, *Tectonophysics,* **622,** 44–55.

Gratier, J.P., Dysthe, D.K. & Renard, F., 2013. The role of pressure solution creep in the ductility of the Earth's upper crust, *Adv. Geophys*., **54,** 47–179.

Gu, J.-C., Rice, J.R., Ruina, A.L. & Tse, S.T., 1984. Slip motion and stability of a single degree of freedom elastic system with rate and state dependent friction, *J. Mech. Phys. Solids,* **32,** 167–196.

Karner, S.L., Marone, C. & Evans, B., 1997. Laboratory study of fault healing and lithification in simulated fault gouge under hydrothermal conditions, *Tectonophysics,* **277,** 41–55.

Logan, J.M. & Rauenzahn, K.A., 1987. Frictional dependence of gouge mixtures of quartz and montmorillonite on velocity, composition and fabric, *Tectonophysics,* **144,** 87–108.

Logan, J.M., Friedman, M., Higgs, M., Dengo, C. & Shimamoto, T., 1979. Experimental studies of simulated gouge and their application to studies of natural fault zones, in *Proceedings of the VIII Conference*, Analysis of Actual Fault Zones, Bedrock, U.S. Geol. Survey, Menlo Park, CA, pp. 305–343.

Lucente, F.P., De Gori, P., Margheriti, L., Piccinini, D., Di Bona, M., Chiarabba, C. & Piana Agostinetti, N., 2010. Temporal variation of seismic velocity and anisotropy before the 2009 MW 6.3 L'Aquila earthquake, Italy, *Geology,* **38,** 1015–1018.

Malagnini, L., Lucente, F.P., De Gori, P., Akinci, A. & Munafo', I., 2012. Control of pore fluid pressure diffusion on fault failure mode: insights from the 2009 L' Aquila seismic sequence, *J. geophys. Res.,* **117,** B05302, doi:10.1029/2011JB008911.

Marone, C., 1998a. Laboratory-derived friction laws and their application to seismic faulting, *Annu. Rev. Earth planet. Sci.,* **26,** 643–696.

Marone, C., 1998b. The effect of loading rate on static friction and the rate of fault healing during the earthquake cycle, *Nature,* **391,** 69–72.

Marone, C., Scholz, C.H. & Bilham, R., 1991. On the mechanics of earthquake afterslip, *J. geophys. Res.,* **96,** 8441–8452.

Miller, S.A., Collettini, C., Chiaraluce, L., Cocco, M., Barchi, M.R. & Kaus, B., 2004. Aftershocks driven by a high pressure CO_2 source at depth, *Nature,* **427,** 724–727.

Mirabella, F., Barchi, M., Lupattelli, A., Stucchi, E. & Ciaccio, M.G., 2008. Insights on the seismogenic layer thickness from the upper crust structure of the Umbriae Marche Apennines (central Italy), *Tectonics,* **27,** 1–15.

Muhuri, S.K., Dewers, T.A., Scott, Jr., T.E. & Reches, Z., 2003. Interseismic fault strengthening and earthquake-slip instability: friction or cohesion?, *Geology,* **31,** 881–884.

Niemeijer, A.R. & Spiers, C.J., 2007. A microphysical model for strong velocity weakening in phyllosilicate-bearing fault gouges, *J. geophys. Res.,* **112,** doi:10.1029/2007JB005008.

Niemeijer, A.R. & Vissers, R.L.M., 2014. Earthquake rupture propagation inferred from the spatial distribution of fault rock frictional properties, *Earth planet. Sci. Lett.,* **396,** 154–164.

Nakatani, M., 2001. Conceptual and physical clarification of rate and state friction: frictional sliding as a thermally activated rheology, *J. geophys. Res.,* **106**(B7), 13 347–13 380.

Noda, H. & Shimamoto, T., 2010. A rate- and state-dependent ductile flow law of polycrystalline halite under large shear strain and implications for transition to brittle deformation, *Geophys. Res. Lett.,* **37,** L09310, doi:10.1029/2010GL042512.

Noda, H. & Shimamoto, T., 2012. Transient behavior and stability analyses of halite shear zones with an empirical rate-and-state friction to flow law, *J. Struct. Geol.,* **38,** 234–242.

Plummer, N.L., Wigley, T.M.L. & Parkhurst, D.L., 1979. Critical review of the kinetics of calcite dissolution and precipitation, in *Chemical Modeling in Aqueous Systems—Speciation, Sorption, Solubility, and Kinetics*, pp. 537–573, ed. Jenne, E.A., Am. Chem. Soc. Symp. Ser., 93.

Putelat, T., Dawes, J.H.P. & Willis, J.R. 2011. On the microphysical foundations of rate-and-state friction, *J. Mech. Phys. Solids,* **59,** 1062–1075.

Reinen, L.A. & Weeks, J.D., 1993. Determination of rock friction constitutive parameters using an iterative least-squares inversion method, *J. geophys. Res.,* **98,** 15 937–15 950.

Renard, F., Beaupretre, S., Voisin, C., Zigone, D., Candela, T., Dysthe, D.K. & Gratier, J.-P., 2012. Strength evolution of a reactive frictional interface is controlled by the dynamics of contacts and chemical effects, *Earth planet. Sci. Lett.,* **341,** 20–34.

Ruina, A., 1983. Slip instability and state variable friction laws, *J. geophys. Res.,* **88,** 10 359–10 370.

Rutter, E.H., 1974. The influence of temperature, strain rate and interstitial water in the experimental deformation of calcite rocks, *Tectonophysics,* **22,** 331–334.

Rutter, E.H., 1983. Pressure solution in nature, theory, and experiment, *J. Geol. Soc. Lond.,* **140,** 725–740.

Rutter, E.H. & Mainprice, D.H., 1979. On the possibility of slow fault slip controlled by a diffusive mass transfer process, *Gerlands Beiträge zur Geophysik,* **88,** 154–162.

Scholz, C.H., 1988. The brittle-plastic transition and the depth of seismic faulting, *Geol. Rundsch.,* **77**(1), 319–328.

Schubnel, A., Walker, E., Thompson, B.D., Fortin, J., Guéguen, Y. & Young, R.P., 2006. Transient creep, aseismic damage and slow failure in Carrara marble deformed across the brittle-ductile transition, *Geophys. Res. Lett.,* **33,** L17301, doi:10.1029/2006GL026619.

Scuderi, M.M., Niemeijer, A.R., Collettini, C. & Marone, C., 2013. Frictional properties and slip stability of active faults within carbonate–evaporite sequences: the role of dolomite and anhydrite, *Earth planet. Sci. Lett.,* **369,** 220–232.

Shimamoto, T., 1986. Transition between frictional slip and ductile flow for halite shear zones at room temperature, *Science*., **231**(4739), 711–714.

Sjöberg, E.L. & Rickard, D.T., 1984. Temperature dependence of calcite dissolution kinetics between 1 and 62°C at pH 2.7 to 8.4 in aqueous solutions, *Geochim. Cosmochim. Acta,* **48,** 485–493.

Sleep, N.H., Richardson, E. & Marone, C., 2000. Physics of friction and strain rate localization in synthetic gouge, *J. geophys. Res.,* **105,** 25 875–25 890.

Smith, S., Nielsen, S. & Di Toro, G., 2015. Strain localization and the onset of dynamic weakening in calcite fault gouge, *Earth planet. Sci. Lett.,* **413,** 25–36.

Takahashi, M., Uehara, S.-I., Mizoguchi, K., Shimizu, I., Okazaki, K. & Masuda, K., 2011. On the transient response of serpentine (antigorite)

gouge to step-wise changes in slip velocity under high-temperature conditions, *J. geophys. Res.,* **116,** B10405, doi:10.1029/2010JB008062.
Tesei, T., Collettini, C., Barchi, M.R., Carpenter, B.M. & Di Stefano, G., 2014. Heterogeneous strength and fault zone complexity of carbonate-bearing thrusts with possible implications for seismicity, *Earth planet. Sci. Lett.,* **408,** 307–318.
Trippetta, F., Mollo, S., Carpenter, B.M. & Collettini, C., 2013. The relationship between fault Zone processes and physical-transport properties: the carbonate-bearing Monte Maggio Fault (Central Italy), in *Proceedings of the 2013 AGU Fall Meeting, Abstract T53C-2591*, 2013 December 9–13, AGU, San Francisco, CA.
Tse, S.T. & Rice, J.R., 1986. Crustal earthquake instability in relation to the depth variation of frictional slip properties, *J. geophys. Res.,* **91,** 9452–9472.
Valoroso, L., Chiaraluce, L. & Collettini, C., 2014. Earthquakes and fault zone structure, *Geology,* **42**(4), 343–346.
Verberne, B.A., He, C. & Spiers, C.J., 2010, Frictional properties of sedimentary rocks and natural fault gouge from the Longmenshan Fault Zone, Sichuan, China, *Bull. seism. Soc. Am.,* **100,** 2767–2790.
Verberne, B.A., De Bresser, J.H.P., Niemeijer, A.R., Spiers, C.J., De Winter, D.A.M. & Plümper, O., 2013. Nanocrystalline slip zones in calcite fault gouge show intense crystallographic preferred orientation: crystal plasticity at sub-seismic slip rates at 18–150°C, *Geology,* **41,** 863–866.
Verberne, B.A., Plümper, O., De Winter, D.A.M. & Spiers, C.J., 2014a. Superplastic nanofibrous slip zones control seismogenic fault friction, *Science,* **346,** 1342–1344.
Verberne, B.A., Spiers, C.J., Niemeijer, A.R., De Bresser, J.H.P., De Winter, D.A.M. & Plümper, O., 2014b. Frictional properties and microstructure of calcite-rich fault gouges sheared at sub-seismic sliding velocities, *Pure appl. Geophys.,* **171,** 2617–2640.
Verberne, B.A., De Bresser, J.H.P., Niemeijer, A.R. & Spiers, C.J., 2015. Mechanical behavior and microstructure of simulated calcite fault gouge sheared at 20–600 °C: implications for natural faults in limestones, *J. geophys. Res.,* doi:10.1002/2015JB012292.
Violay, M., Nielsen, S., Spagnuolo, E., Cinti, D., Di Toro, G. & Di Stefano, G., 2013. Pore fluid in experimental calcite-bearing faults: abrupt weakening and geochemical signature of co-seismic processes, *Earth planet. Sci. Lett.,* **361,** 74–84.
Weeks, J.D. & Tullis, T.E., 1985. Frictional sliding of dolomite: a variation in constitutive behaviour, *J. geophys. Res.,* **90,** 7821–7826.
Zhang, X. & Spiers, C.J., 2005. Compaction of granular calcite by pressure solution at room temperature and effects of pore fluid chemistry, *Int. J. Rock Mech. Min. Sci*., **42,** 950–960.

SUPPORTING INFORMATION

Additional Supporting Information may be found in the online version of this paper:

Table S1. Calculated rates and their coefficient of determination (R^2) values for a logarithmic fit to all data points.
Figure S1. SEM images of the starting material used in this study. Material was loaded to 5 MPa normal stress under 5% RH conditions, and then sampled for thin section.
Figure S2. SEM images for experiments performed at 0.3 μm s^{-1} (top panel) and 3000 μm s^{-1}. Images show no major differences between the shown velocities.
(http://gji.oxfordjournals.org/lookup/suppl/doi:10.1093/gji/ggw038/-/DC1).

Please note: Oxford University Press is not responsible for the content or functionality of any supporting materials supplied by the authors. Any queries (other than missing material) should be directed to the corresponding author for the paper.